

Interrogating the Mechanistic Features of Ni(I)-Mediated Aryl Iodide Oxidative Addition Using Electroanalytical and Statistical Modeling Techniques

Tianhua Tang,^{||} Avijit Hazra,^{||} Daniel S. Min, Wendy L. Williams, Eli Jones, Abigail G. Doyle,^{*} and Matthew S. Sigman^{*}



Cite This: <https://doi.org/10.1021/jacs.3c01726>



Read Online

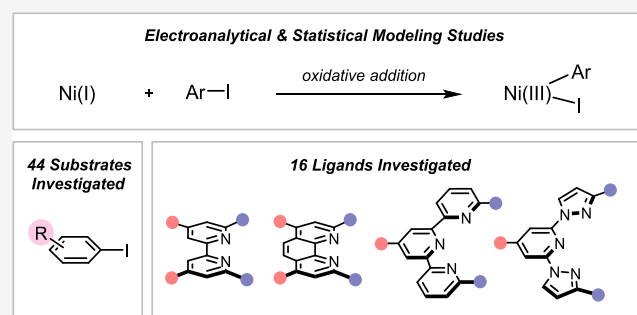
ACCESS |

Metrics & More

Article Recommendations

Supporting Information

ABSTRACT: While the oxidative addition of Ni(I) to aryl iodides has been commonly proposed in catalytic methods, an in-depth mechanistic understanding of this fundamental process is still lacking. Herein, we describe a detailed mechanistic study of the oxidative addition process using electroanalytical and statistical modeling techniques. Electroanalytical techniques allowed rapid measurement of the oxidative addition rates for a diverse set of aryl iodide substrates and four classes of catalytically relevant complexes (Ni(^{Me}BPy), Ni(^{Me}Phen), Ni(Terpy), and Ni(BPP)). With >200 experimental rate measurements, we were able to identify essential electronic and steric factors impacting the rate of oxidative addition through multivariate linear regression models. This has led to a classification of oxidative addition mechanisms, either through a three-center concerted or halogen-atom abstraction pathway based on the ligand type. A global heat map of predicted oxidative addition rates was created and shown applicable to a better understanding of the reaction outcome in a case study of a Ni-catalyzed coupling reaction.



INTRODUCTION

In the past 10 years, tremendous progress has been reported in the functionalization of aryl halides using nickel catalysis to form C–C and C–heteroatom bonds.^{1–7} An essential mechanistic event in these transformations is the oxidative addition of the aryl halide, typically mediated by a low-valent nickel complex (Figure 1A).¹ While Ni(0) has been implicated in traditional variations of these cross-coupling reactions,^{8–10} Ni(I) species supported by bi- and tridentate nitrogen-based ligands have frequently been proposed in modern variants such as Ni-catalyzed cross-electrophile coupling, Ni/photoredox catalysis, and Ni electrocatalysis.^{11–17} Seminal organometallic studies by numerous groups have demonstrated the viability of such a step with Ni(I) complexes bearing *N*-heterocyclic carbene,^{18,19} bipyridine,^{15,20–23} phenanthroline,²⁴ pyridine-oxazoline,²⁵ bis-oxazoline,²⁶ and other nitrogenous ligands^{27,28} (Figure 1B). The Doyle group recently conducted a detailed investigation with a tailored Ni(I)-bipyridine complex, providing direct evidence of the Ni(III)-aryl species resulting from Ni(I) oxidative addition.²⁰ Kinetics, linear free-energy relationships, and other stoichiometric studies were conducted to evaluate the mechanism of oxidative addition with this metal–ligand system.

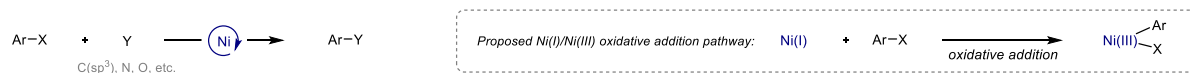
While these prior studies have revealed key mechanistic features of Ni(I) oxidative addition, the studies were focused on a limited subset of nitrogen-based ligands due to the

limitations in synthetic methods to access Ni(I) and the instability of the catalytically relevant three-coordinate Ni(I) complex. In addition, the propensity of Ni(I) to undergo complex speciation convolutes mechanistic analysis.^{20,22} Given the variety of substrates and ligands now used in nickel(I) catalysis, a broader survey of how these critical variables impact the oxidative addition mechanism would provide a valuable foundation for developing new and improved catalytic transformations. To this end, we became interested in determining the mechanistic generalities of oxidative addition in regard to other commonly utilized bi- and tridentate nitrogen-based ligand/Ni(I) complexes with the goal of identifying how ligand and substrate features impact the process.^{29–31}

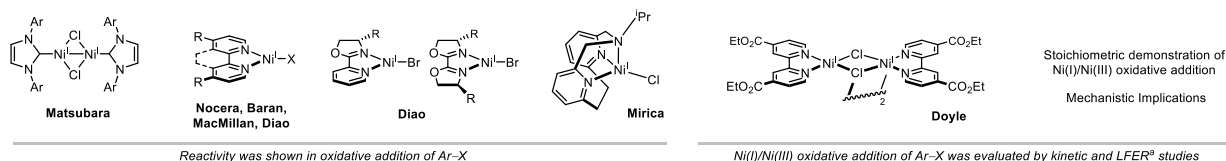
To address these challenges, our group^{33–38} and others³² have recently established an approach to study oxidative addition mechanisms by combining electroanalytical techniques with data science tools. Specifically, the in situ generation

Received: February 17, 2023

A. Synthetic Relevance of Aryl Halide Oxidative Addition to Ni(I)



B. Preceding Studies: Organometallic Approaches



C. This Work: Electroanalytical Approach & Statistical Modeling Studies

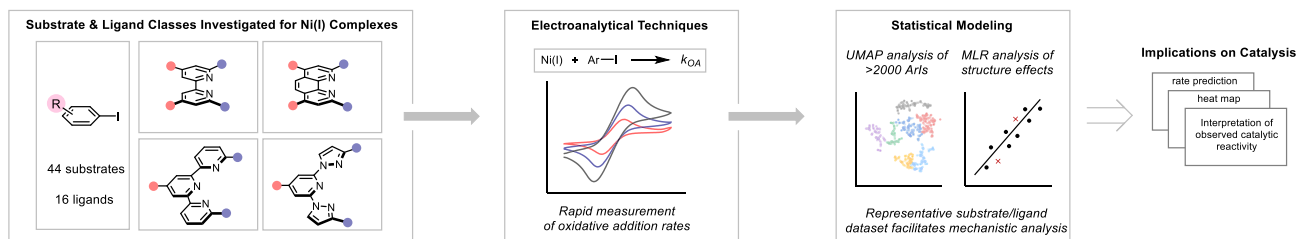


Figure 1. (A) Ni(I) oxidative addition and its synthetic applications. (B) Previous oxidative addition studies of aryl halides by Ni(I) complexes through organometallic approaches. (C) Current study on oxidative addition of aryl iodides by Ni(I) complexes, including the substrate/ligand library, electroanalytical and statistical modeling workflow, and mechanistic implications from this work. ^aLFER: linear free-energy relationship.

of low-valent metal complexes by cathodic reduction avoids the difficulties associated with the isolation and characterization of the complexes and allows for rapid exploration of diverse ligands. Furthermore, the facile acquisition of kinetic data using electrochemistry enables the evaluation of a wide range of substrates. This, in turn, feeds data science methods to build statistical models correlating structure to function.^{32–38} Given these advantages, we were optimistic that this electroanalytical approach would allow us to interrogate the structural features of ligands and substrates that impact the mechanism of oxidative addition of Ni(I) complexes.

Herein, we present a general investigation of aryl iodide oxidative addition using electrochemically formed Ni(I) complexes of four representative classes of catalytically relevant ligands (MeBPy, 6,6'-dimethyl-2,2'-bipyridine; MePhen, neocuproine; Terpy, terpyridine; BPP, 2,6-bis((1H-pyrazol-1-yl)methyl)pyridine, Figure 1C). Electroanalytical techniques allowed for the rapid measurement of oxidative addition rates of 44 aryl iodides with 16 unique ligands. Traditional physical organic analysis tools combined with modern data science techniques were employed to probe the structure–activity relationships of this key step. This ultimately has led to predictive models for oxidative addition using Ni(I) complexes. Finally, in a case study, we show how these models can be used in mechanistic studies of catalytic reactions that are proposed to proceed via Ni(I) oxidative addition to aryl iodides.

RESULTS AND DISCUSSION

Electroanalytical Studies of the Ni(I) Complexes and Their Reactivity with Aryl Iodides. Our group^{33–38} and others³² have reported an electroanalytical approach to study oxidative addition processes involving low-valent first-row transition metals into alkyl electrophiles. The rate of oxidative addition is measured using cyclic voltammetry through peak-ratio analysis. Specifically, rate constants were calculated by

varying the scan rates and relating the variation of scan rates to the change of peak ratios of the metal species, which reflects the depletion in the metal species' concentration. (See the Supporting Information for a more detailed discussion.) In prior studies, we have applied this method to study the oxidative addition processes of activated sp³ electrophiles such as benzyl halides^{34–36} and allyl electrophiles.³⁸ However, this method is yet to be applied to the reaction of aryl electrophiles.

As bidentate and tridentate nitrogenous ligands are the most commonly used in modern variants of Ni-catalyzed coupling reactions of aryl electrophiles, we selected representative achiral examples³⁹ for evaluation, including bipyridine (BPy),^{15,16,40–44} phenanthroline (Phen),^{17,24,45–47} terpyridine (Terpy),^{48–50} and 2,6-bis((1H-pyrazol-1-yl)methyl)pyridine (BPP)-type ligands.^{51,52}

We began our study by conducting cyclic voltammetry (CV) measurements of the Ni(II)/Ni(I) redox couple of prepared Ni(II) complexes containing BPy, Phen, Terpy, and BPP ligands. However, Ni complexes bearing the parent bidentate ligands, bipyridine, and phenanthroline resulted in uninterpretable CVs with overlapping peak responses, consistent with literature precedent.^{15,24} This is likely due to speciation processes by Ni(II) and disproportionation processes by Ni(I),¹⁵ which prevent further application of this technique for quantitative analysis. Inspired by previous reports,^{38,53} we hypothesized that placing methyl groups adjacent to the nitrogen atoms of the ligands could minimize speciation issues and stabilize the nickel center from undesired disproportionation reactions through steric shielding of the metal center. Indeed, we found that MeBPy (6,6'-dimethyl-2,2'-bipyridine) and MePhen (neocuproine) were effective ligands and provided interpretable CVs for the nickel complexes. Although modification of the ligand is required, MeBPy,^{16,41,44,54} and MePhen^{17,24,45,55} ligands have demonstrated catalytic reactivity for processes that undergo oxidative addition of aryl halides. Interestingly, the modification was not necessary for tridentate

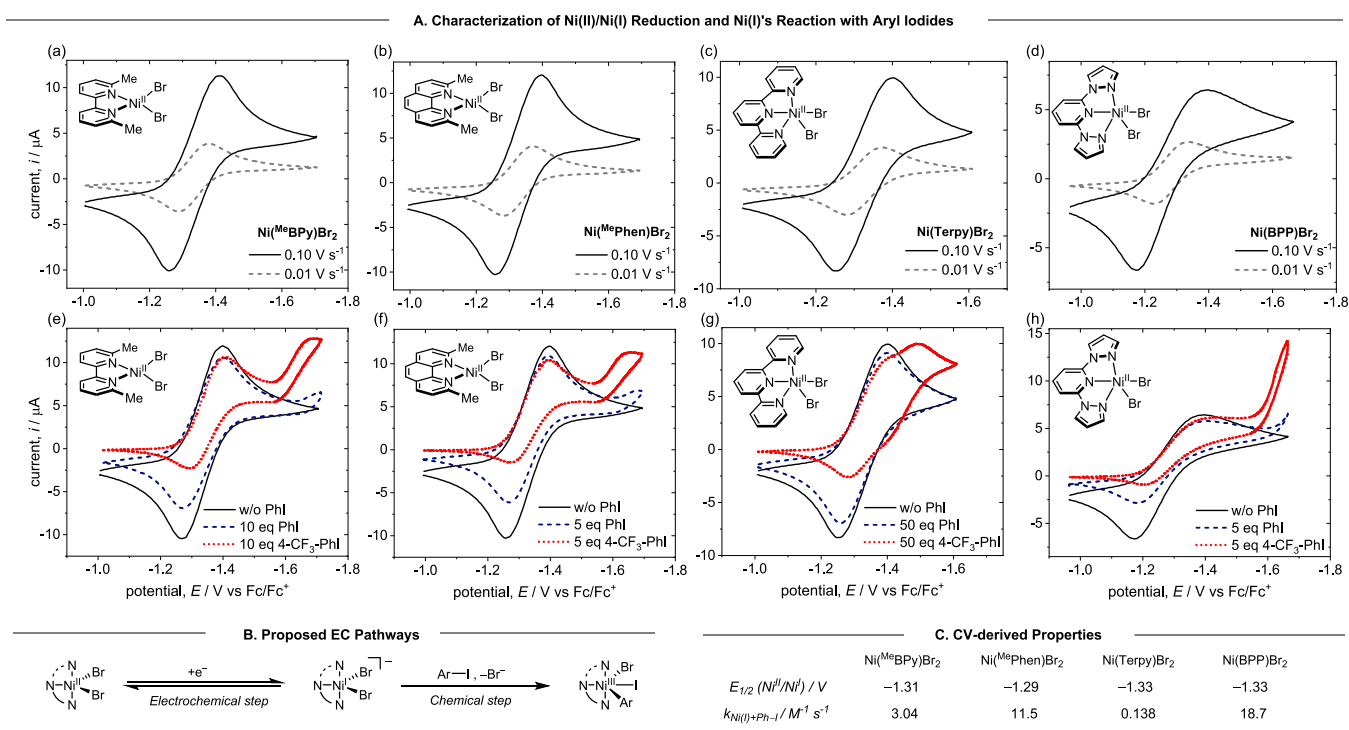


Figure 2. (A) Representative reversible cyclic voltammograms of 1.0 mM-synthesized (a) Ni(^{Me}BPY)Br₂, (b) Ni(^{Me}Phen)Br₂, (c) Ni(Terpy)Br₂, and (d) Ni(BPP)Br₂. (e–h) CV with addition of aryl halides (concentration specified in the figure). All CVs run at scan rates of 0.10 or 0.01 V/s in a 100 mM solution of TBABr in DMA, using a 0.071 cm² boron-doped diamond working electrode. All CVs are from the second scan. (B) Proposed EC pathways. (C) Redox potentials and rate constants (with Ph–I) tabulated for each complex.

ligands such as Terpy and BPP, possibly due to the increased coordinative saturation. It should be noted that the speciation of these Ni complexes is often sensitive to the reaction conditions and can vary. Although our CV studies indicate formation of the mono-ligated nickel complexes, it is crucial to exercise caution when evaluating different analytical scenarios or during a catalytic reaction. Furthermore, care should be taken when translating the mechanistic outcomes of the ^{Me}BPY/^{Me}Phen systems to Ni-catalyzed methods that rely on unmodified bipyridine or phenanthroline ligands.

Further evaluation of the CV conditions revealed that *N,N*-dimethylacetamide (DMA) as a solvent and tetrabutylammonium bromide (TBABr) as the supporting electrolyte proved most effective (for other solvent/electrolyte conditions, see the Supporting Information, Section 3). The observed influence of the solvent and electrolyte could potentially be attributed to influences on the coordination environment of the Ni complexes. A boron-doped diamond electrode with a high overpotential for hydrogen evolution (−1.5 V in H₂O) was used for this analysis. Figure 2A(a–d) depicts the CVs of the synthesized Ni(^{Me}BPY)Br₂, Ni(^{Me}Phen)Br₂, Ni(Terpy)Br₂, and Ni(BPP)Br₂ complexes, measured at the scan rates of 0.10 and 0.01 V s^{−1}. Excellent Ni(II)/Ni(I) reversible couples at both scan rates were observed for all four complexes, which allowed us to perform further analysis.

Next, we investigated the reactivity of the transiently generated Ni(I) complexes with aryl iodide substrates using CV [Figure 2A(e–h)]. Upon the addition of multiple equivalents of phenyl iodide, the cyclic voltammograms (blue dashed trace) for all four Ni complexes exhibited a loss of reversibility: a noticeable change in the return peak current was observed in all cases. This is consistent with the interception of electrogenerated Ni(I) species by phenyl iodide, indicative of

an oxidative addition process.^{15,34–38} A more electrophilic substrate, 4-CF₃-phenyl iodide, was used to validate this process. As is depicted in Figure 2A(e–h) (red dotted trace), a significant loss of reversibility was observed, indicating a more facile oxidative addition than that observed for phenyl iodide. A similar effect of aryl halide electrophilicity on Ni(I)'s oxidative addition was observed in previous reports using pulse radiolysis²² and stoichiometric studies.²⁰

Moreover, we observed the generation of a new species in all CVs [highlighted in red bold, Figure 2A(e–h)]. We hypothesized that this new species could be a Ni^{II}(aryl) species, a resting-state intermediate previously observed in Ni(I)'s oxidative addition of aryl halides, presumably formed by a subsequent reduction of the resulting Ni^{III}(aryl) species at the electrode.^{20,25,26,56} The observed oxidative addition process was slower for the Ni^I(Terpy) complex, requiring a larger excess of aryl iodide (50 equiv). As a result, the CV patterns for these Ni complexes can be interpreted as an EC-type mechanism (electrochemical reduction, “E,” followed by a chemical step of Ni(I)'s oxidative addition into aryl iodide, “C,” Figure 2B).

The rate constants for the chemical step in the EC mechanism were determined using peak-ratio analysis.^{32–38} The ratios of forward and return peak currents were measured using CV for Ni complexes and phenyl iodide at different scan rates. The rate constants were subsequently obtained by correlating the peak ratios and scan rates. The readers are directed to the Supporting Information (Section 2) for a more detailed discussion. Consistent with the qualitative analysis, the oxidative addition rate is faster for Ni^I(^{Me}Phen) and Ni^I(BPP) than Ni^I(^{Me}BPY); the Ni^I(Terpy) complex reacted the slowest with phenyl iodide (>20 times slower than the others) (Figure 2C).

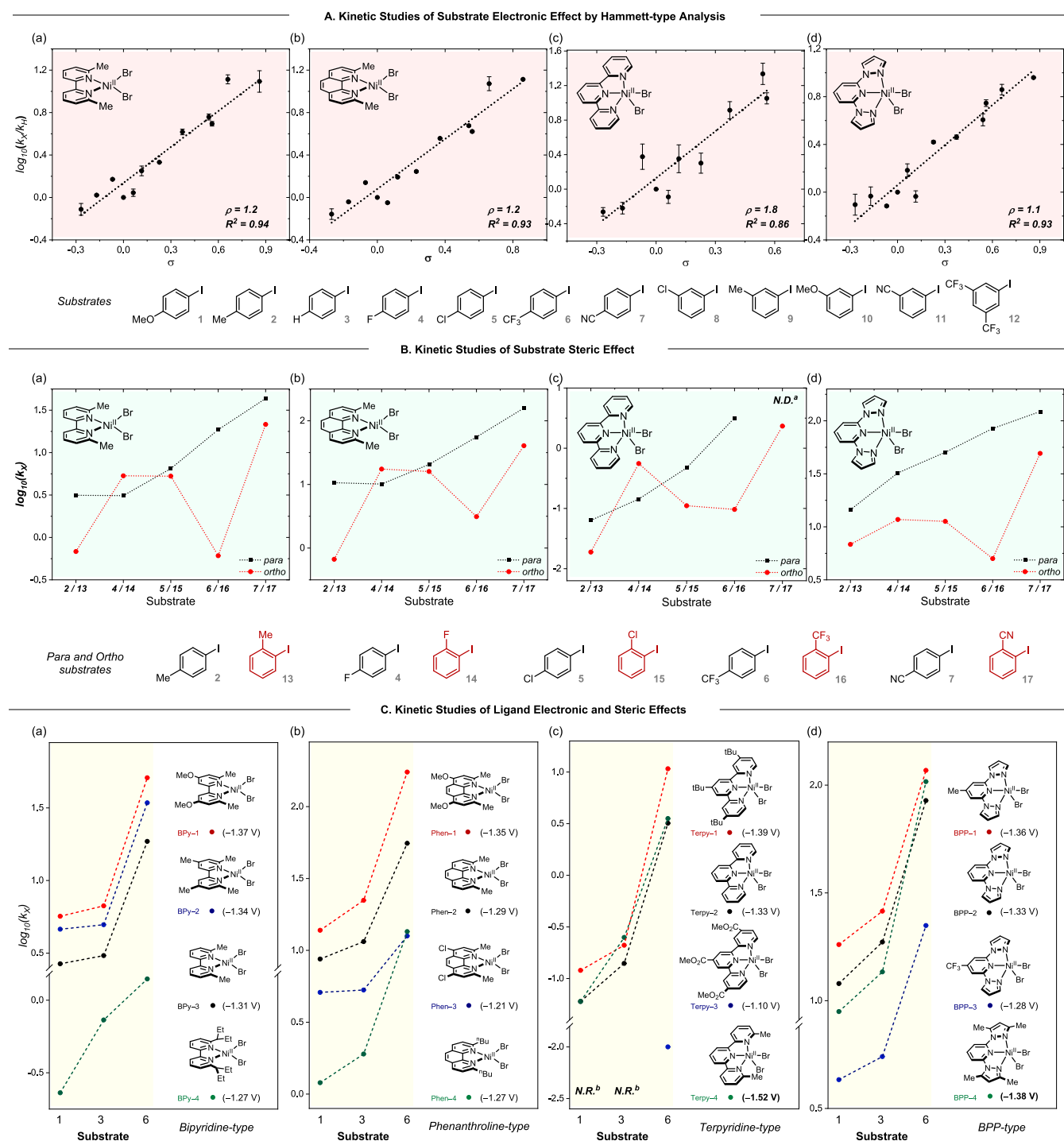


Figure 3. (A) Linear free-energy relationship (Hammett-type) studies of oxidative addition reactions with all Ni complexes: correlation of σ parameters to kinetic data from Ni complexes specified in (a–d). (B) Kinetic studies of the substrate steric effect. (C) Kinetic studies of ligand electronic and steric effects. Measured redox potential (vs Fc/Fc⁺) for each Ni complex is depicted in parentheses. ^aN.D.: rate constant with substrate 7 not determined due to complete loss of reversibility on CV. ^bN.R.: no observation of oxidative addition with substrate 1 and 3 using Terpy-3 ligand.

Kinetic Studies of Substrate and Ligand Electronic and Steric Effects. As the next step, we conducted a linear free-energy relationship (Hammett-type) study to investigate the mechanism of oxidative addition.^{34–36,38} Traditional Hammett-type aryl iodide substrates (1–12) bearing electronically diverse substituents on the *para* and *meta* positions were selected. We measured the relative rate constants for all 12

substrates with the four Ni complexes, and the resulting Hammett analysis is summarized in Figure 3A(a–d).⁵⁷ A linear trend with moderately positive ρ values for all complexes was observed, suggesting negative charge build-up on the arene during the oxidative addition process. Of particular note, the ρ values of all complexes are within the range between 1 and 2. This observation is consistent with previous reports by the

Doyle²⁰ and MacMillan²² groups, where ρ values for the oxidative addition of Ni(I) complexes supported by bipyridine-type ligands were determined to be 1.07 and 1.3, respectively.

From previous studies of aryl halide oxidative addition, four possible pathways were proposed and can be distinguished by their Hammett ρ values. These pathways include nucleophilic aromatic substitution (S_NAr , $\rho \sim 4$),⁵⁸ single-electron transfer ($\rho \sim 5$),⁵⁹ three-center concerted ($\rho \sim 2$),⁶⁰ and halogen-atom abstraction ($\rho \sim 1$),⁶¹ depicted in Figure 4. The observed Hammett ρ values in our study are most consistent with either a three-center concerted or halogen-atom abstraction pathway.

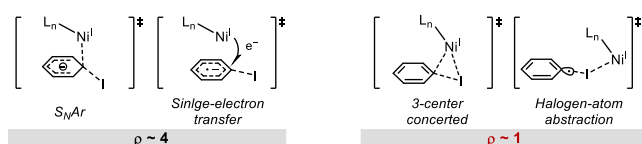


Figure 4. Hammett ρ values reported for oxidative addition pathways.

As a next step, we explored how steric effects impacted the oxidative addition rate by comparing *ortho*-substituted substrates 13–17 to their *para*-substituted analogues. Faster rates were observed for *para*-substituted substrates [black circles in Figure 3B(a–d)] than that of *ortho*-substituted substrates [red circles in Figure 3B(a–d)] with the notable exception of fluorinated substrates (4 and 14). The sensitivity to steric hindrance is consistent with inner-sphere processes such as three-center concerted or halogen-atom abstraction mechanisms, which are expected to have a greater steric dependence compared to an outer-sphere electron transfer.⁶² Similar steric effects on oxidative addition rates were also observed by the Doyle group for *ortho*-methylated phenyl

bromides.²⁰ Deviation from this trend by fluorinated substrates could be due to the smaller size of the fluorine atom. We also observed that for the ^{Me}BPy, ^{Me}Phen, and Terpy systems [Figure 3B(a–c)], substrate 14 exhibits a faster reaction rate than substrate 4. However, the opposite trend was observed for the BPP systems [Figure 3B(d)]. We speculate that this may suggest different operating mechanisms between the ^{Me}BPy, ^{Me}Phen, and Terpy systems and the BPP systems, as revealed by the statistical modeling studies (vide infra).

In this context, we also probed how changes to the ligand structure impacted the reaction rate. This is particularly important because structural features of supporting ligands invariably play a crucial role in rates. Unfortunately, inaccessibility and/or deleterious homodimerization of Ni(I) complexes often hamper direct comparisons using traditional mechanistic methods.^{10,20,32} Four diverse variants were chosen for each class of ligand (BPy, Phen, Terpy, and BPP), and the corresponding Ni(II) complexes were prepared, with their redox potentials measured [recorded in Figure 3C(a–d)]. Rate constants for substrates 1, 3, and 6 were then measured with all 16 Ni complexes, and the data was tabulated (Figure 3C). First, an electronic effect on oxidative addition rates was observed for all ligand types. Electron-rich ligands (BPy-1–2, Phen-1, Terpy-1, and BPP-1) accelerated the oxidative addition for 1, 3, and 6, while Ni(I) complexes with electron-deficient ligands (Phen-3, Terpy-3, and BPP-3) slowed the rates. We also observed inhibition of oxidative addition by sterically demanding ligands (BPy-4 and Phen-4). Interestingly, however, Terpy-4 and BPP-4 ligands bearing *ortho*-methyl substituents did not significantly alter the rates compared to the Terpy-2 or BPP-2 ligands. We believe that this could be due to a balance of opposing electronic and steric

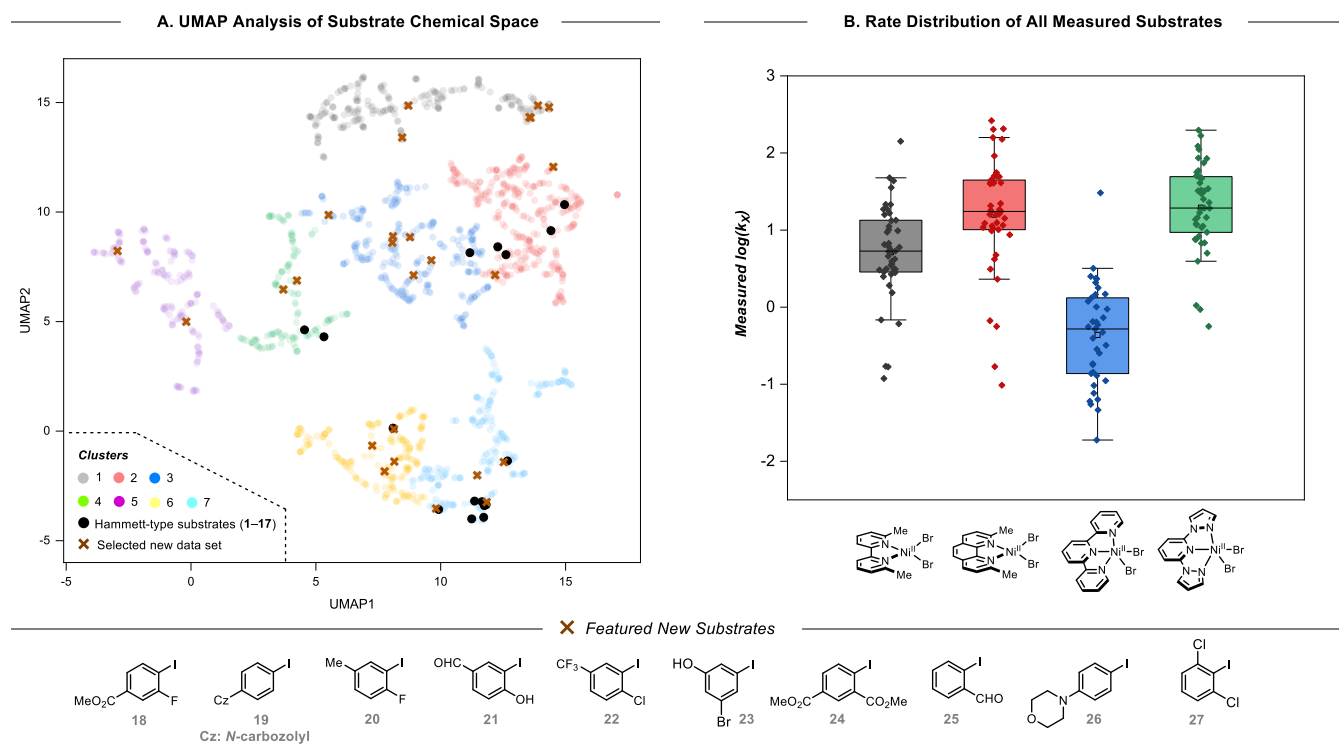


Figure 5. (A) UMAP analysis of 2055 commercial aryl iodide substrates (7 clusters representing different chemical spaces are highlighted by colored circles, black circle: Hammett-type substrates, brown cross: selected new substrates). (B) Distribution of measured oxidative addition rate constants for each of the four Ni(I) complexes. Selected featured new substrates (18–27) are presented at the bottom.

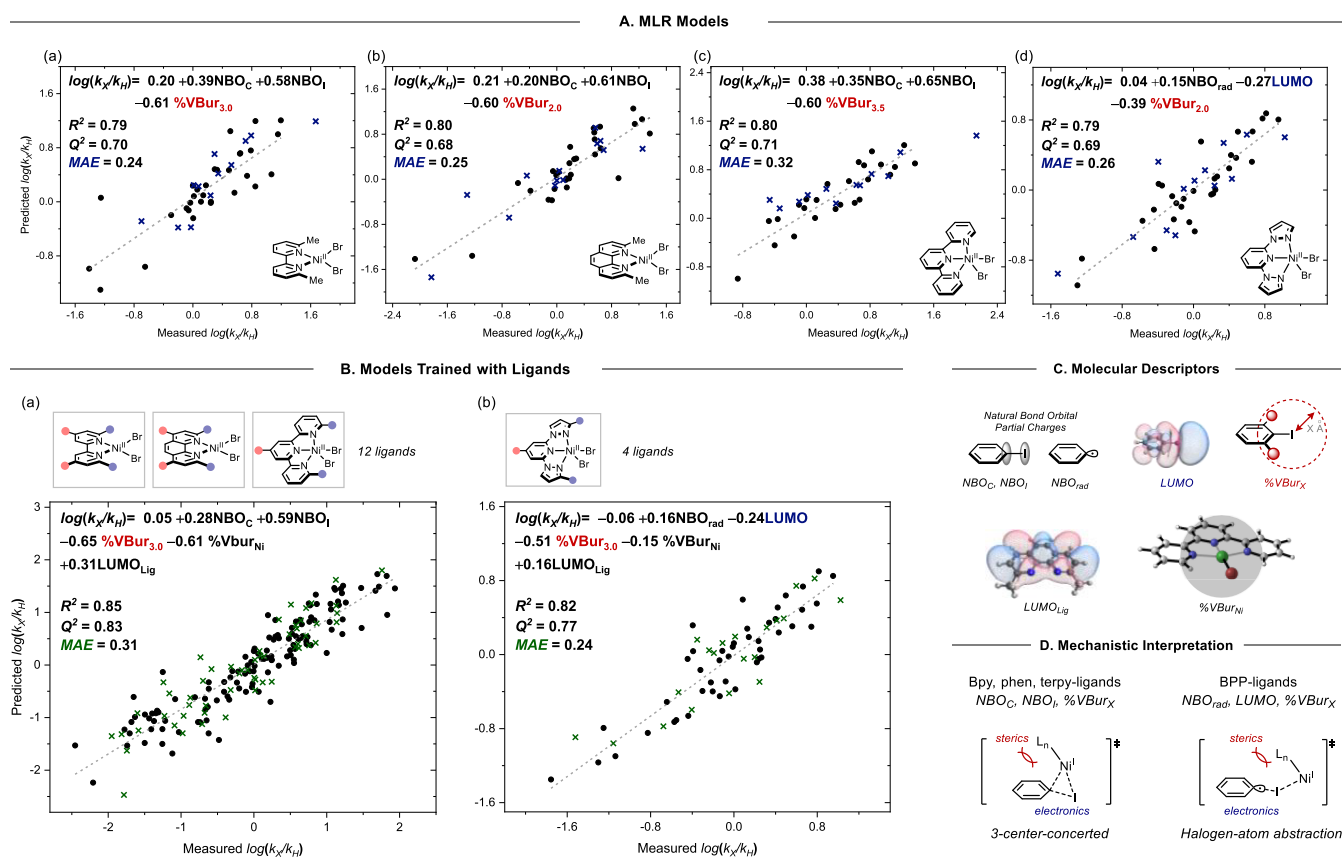


Figure 6. (A) MLR models of all substrates with a pseudo-random 70:30 split in the training/validation data set (black circle: training set, blue cross: validation set). (B) MLR analysis of all kinetic data with a pseudo-random 70:30 split in the training/validation data set (black circle: training set, green cross: validation set). (C) Molecular descriptors used in the models. (D) Mechanistic interpretation.

effects caused by the *ortho*-methyl groups. The redox potentials of the Terpy-4 (−1.52 V) and BPP-4 (−1.38 V) complexes indicate that they are more electron-rich than the Terpy-2 and BPP-2 (both −1.33 V) complexes. This favorable electronic effect causes the Terpy-4 and BPP-4 complexes to be more effective in oxidative addition. Hence, the methyl groups function as both electron-donating groups (which facilitate oxidative addition) and sterically hindered groups (which retard oxidative addition). These two effects seemingly counteract each other, resulting in similar oxidative addition rates between the Terpy-4/Terpy-2 or BPP-4/BPP-2 ligands.

Interrogation of Mechanisms through Statistical Modeling. To generalize this analysis to a broader range of substrates (not simple Hammett-type substitution of arenes), we conducted a multivariate linear regression (MLR) analysis on the four representative Ni complexes.^{63,64} The MLR workflow has two essential components: (1) acquisition of rate data for a diverse set of substrates and/or ligands and (2) extraction of structural properties from DFT computed molecular parameters. Statistical models with a correlation between experimental rate constants and DFT computed parameters can then be constructed and utilized to interpret the mechanism or provide a predictive platform.

Analysis of the Chemical Space of the Aryl Iodides by UMAP. To ensure the diversity of substrates and determine an appropriate dataset for the MLR studies, we surveyed the substrate chemical space by analyzing a range of DFT parameters for a database of 2055 commercial aryl iodides applying uniform manifold approximation and projection

(UMAP) analysis for dimensionality reduction (to reduce the high dimensional DFT features to a two-dimensional plot of chemical space).⁶⁵ This results in a graphical depiction of the property space in which an aryl iodide is similar to the other substrates in the same vicinity.⁶⁷ For more details on the UMAP development, we direct readers to the [Supporting Information](#) (Section 11).

We next employed a hierarchical clustering algorithm to group similar aryl iodides into classes based on their DFT features. In doing so, we incorporated both global features (such as dipole, electronegativity, highest occupied molecular orbital energy, lowest unoccupied molecular orbital energy, etc.) and atomic features (such as NMR shifts, partial charges, and buried volumes of critical atoms), with collinear or low-variance features removed from this analysis. We identified seven clusters for the commercially available aryl iodides, as shown in [Figure 5A](#). To cover the entire property space in the UMAP representation and complement the original substrate set (1–17, black circles) used in Hammett-type studies ([Figure 3](#)), we added 27 new substrates (brown crosses) from the unoccupied space (18–27 as representatives). Indeed, the new substrates exhibit more diverse structural features, such as trisubstituted (18, 20, 21, 22, and 23), N-functionalized (19 and 26), *ortho*-carbonyl-substituted (24 and 25), and *ortho*-disubstituted (27) substrates, which were not present in our initial Hammett-type set (1–17).

We measured the oxidative addition rates of the new substrates with all four Ni(I) complexes. In [Figure 5B](#), we compared the rate-constant distribution across different aryl

iodides between different complexes using a boxplot. In general, Ni^I(^{Me}Phen) and Ni^I(BPP) complexes showed the highest reactivity. Ni^I(^{Me}BPy) complexes, in contrast, underwent oxidative addition more slowly compared to the Ni^I(^{Me}Phen) and Ni^I(BPP) complexes, whereas the Ni^I(Terpy) is a significantly slower complex to activate the aryl iodide. The rate distribution could also explain why BPP, Phen, and BPy nickel complexes are more prevalent in catalysis than the terpyridine complexes.

Parameterization of Substrates and MLR Modeling of the Kinetic Data. With the experimental rate data collected for the UMAP-guided substrate set, we turned to MLR modeling. Based on the proposal of a three-center concerted and halogen-atom abstraction-type mechanism for oxidative addition (Figure 4), we hypothesized that parameters which describe charge stabilization and/or local steric effects would be crucial to building interpretable statistical models. These parameters include natural bond orbital (NBO) charges on the aryl iodide substrate and the aryl radical intermediate (the intermediate formed after halogen-atom abstraction), lowest unoccupied molecular orbital (LUMO) energy, and percent buried volume (% VBur) encompassing the iodine atom.⁶⁶

A pseudo-random split of the data into training and validation sets (70:30 split) was performed on the entire data set. Applying a forward stepwise multivariate regression algorithm, statistical models correlating the rate data with the DFT parameters for each complex were found with good correlation statistics ($R^2 \sim 0.8$, $Q^2 \sim 0.7$, leave-one-out validation, Figure 6A). The generalizability in these models was validated by the withheld test set (blue cross) with mean absolute errors (MAEs) of less than 0.32 for $\log(k_X/k_H)$. As shown in Figure 6A(a–d), for Ni(^{Me}BPy), Ni(^{Me}Phen), and Ni(Terpy) systems, oxidative addition rates were found to correlate with three substrate parameters: (1) NBO_C: NBO charge on the aryl carbon connected to iodine; (2) NBO_I: NBO charge on the iodine; (3) % VBur_{2.0}, % VBur_{3.0}, or % VBur_{3.5}: percentage buried volume centered at iodine measured with a radius of 2.0 (Ni(^{Me}Phen)), 3.0 (Ni(^{Me}BPy)), or 3.5 (Ni(Terpy)) Å. In contrast, for the Ni(BPP) model, NBO_{rad} (NBO charge on the radical carbon of the aryl radical intermediate), LUMO energy for substrates, and % VBur_{2.0} parameters were found to describe oxidative addition rates. The requirement for different parameters in the Ni(BPP) system suggests that this Ni(I) complex proceeds by a distinct oxidative addition pathway from the other three complexes (vide infra). All parameters used in this study are depicted in Figure 6C.

Effect of Ligands on Oxidative Addition. Electronic and steric modifications of ligands often play a significant role in the oxidative addition process, which has been well documented.^{29–31} However, a systematic study to elucidate the role of structural modifications of ligands in Ni(I) mediated oxidative addition of aryl halides has not been disclosed. Therefore, we questioned if we could use this workflow to interrogate ligand structure–activity relationships in this process. Rate data were measured and modeled by combining BPy, Phen, and Terpy complexes. The Ni^I(BPP) complexes were modeled separately based on our finding that these complexes likely undergo oxidative addition via a different mechanism. Inspired by our study in Figure 3C, we hypothesized that global electronic and/or steric parameters from the ligand or Ni(I) complex would capture the rate trends observed for the different ligands. Indeed, as shown in Figure

6B(a), the kinetic data from 12 Ni complexes bearing modified ligands (^{Me}BPy, ^{Me}Phen, and Terpy-type ligands) were found to correlate to three substrate parameters, one ligand parameter, and one parameter from the Ni(I) complexes (Figure 6C): (1) three substrate parameters are consistent with those used in Figure 6A(a–c); (2) LUMO_{Lig}: LUMO energy of the ligand; (3) % VBur_{Ni}: percentage buried volume centered at Ni(I) with a radius of 3 Å. Figure 6B(b) shows a good correlation for four Ni complexes bearing BPP-type ligands. This model used three substrate parameters similar to those used in Figure 6A(d) (NBO_C, LUMO, and % VBur_{3.0}) and the same two catalyst parameters (% VBur_{Ni} and LUMO_{Lig}). These two modeling studies were both conducted using a 70:30 training and validation split and achieved good correlation statistics ($R^2 \sim 0.8$, $Q^2 \sim 0.8$, black circles), which were validated by the test set (green cross in both models) with an MAE of 0.31 or 0.24, respectively.

Analysis of Oxidative Addition Based on Statistical Models. Our mechanistic interpretation of these parameters in the MLR models (Figure 6A,B) is summarized below:

- (1) Ni(^{Me}BPy), Ni(^{Me}Phen), and Ni(Terpy): The positive correlation with the aryl iodide NBO_C and NBO_I indicates negative charge build-up on these two atoms during the transition state. This is consistent with an orbital interaction between Ni(I) and these two atoms during oxidative addition. Therefore, the correlation with these two parameters, seen in Ni(^{Me}BPy), Ni(^{Me}Phen), and Ni(Terpy)'s models [Figure 6A(a–c) and B(a)], suggests a three-center concerted pathway depicted in Figure 6D, which is consistent with prior Hammett-type studies.²⁰
- (2) The positive correlation with NBO_{rad} (from aryl radical intermediate) in Figure 6A(d) and B(b) suggests the intermediacy of an *ipso*(aryl) radical during the oxidative addition process. The negative correlation with the LUMO of aryl iodides indicates an electron transfer process. These findings, combined with the moderate ρ value [1.1, Figure 3A(d)] in the Hammett study, suggest a halogen-atom abstraction-type mechanism for the oxidative addition by Ni(BPP) complexes (depicted in Figure 6D).
- (3) The negative correlation with % VBur parameters on the substrates and Ni(I) complex in all models indicates an impact of steric effects that is most consistent with inner-sphere oxidative addition mechanisms.⁶⁸
- (4) The correlation with the LUMO_{Lig} parameter characterizes the electronic impact of the ligand on oxidative addition rates of Ni(I). A higher LUMO energy of the ligand is associated with a faster rate as it leads to a more electron-rich Ni(I) center, possibly due to weaker back-bonding from Ni(I) to the ligand. This is supported by the observation that Ni^I(^{Me}BPy) and Ni^I(^{Me}Phen) have faster oxidative addition rates than Ni^I(Terpy) because these two bidentate ligands support a more electron-rich Ni center than the tridentate ligand. A similar interpretation can be applied to the Ni^I(BPP) system [Figure 6B(b)], albeit a different mechanism is proposed. This is in line with our observation of ligand electronic effects in Figure 3C.

Implications in Catalysis. The statistical models developed can be utilized to quantitatively predict the oxidative addition rate for out-of-sample aryl iodides. We anticipated

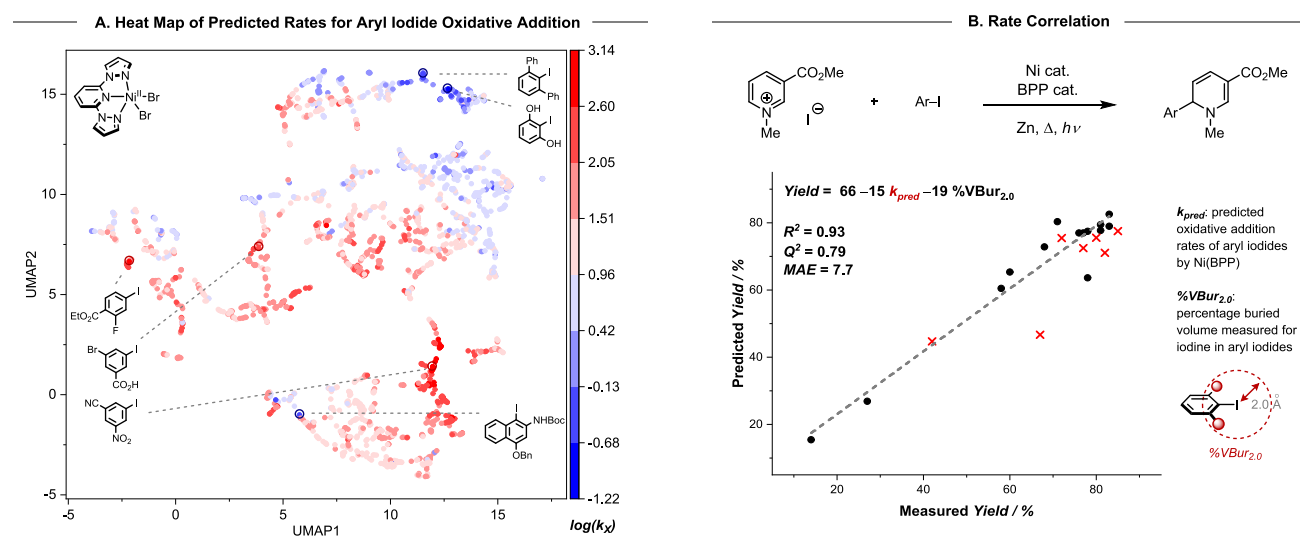


Figure 7. (A) Heat map plot of predicted oxidative addition rate across 2055 commercially available aryl iodides (the color represents rates: dark red represents fast rates and dark blue represents slow rates). (B) Statistical modeling study of a Ni-catalyzed cross-coupling of pyridinium salts and aryl iodides was conducted with a correlation between yields⁵² and parameters (depicted in the figure).

that this could be useful in new reaction development and reaction scope analysis as quantitative knowledge of the critical oxidative step in catalysis could be utilized to understand catalytic reactivity. Accordingly, using the DFT features of 2055 commercially available aryl iodides in Figure 5A and our MLR model in Figure 6A(d), we estimated their rates of oxidative addition with Ni(BPP), resulting in the heat map shown in Figure 7A. We found that aryl iodides with high, moderate, and low oxidative addition rates tend to cluster together, suggesting that the structural features used for the chemical space analysis also capture reactivity features. For example, a closer evaluation of areas of extreme reactivity shows that 2,6-substituted substrates clustered in an unreactive region of the chemical space and substrates with multiple electron-withdrawing functionalities clustered in regions of higher reactivity.

Using these predicted oxidative addition rates, we set out to evaluate their utility for predicting reaction outcomes and mechanistic analysis in catalysis. We selected a Ni(BPP)-catalyzed cross-coupling reaction between pyridinium salts and aryl iodides, reported by Karimov et al., as a case study.⁵² This reaction was analyzed for two reasons: first, it is proposed to proceed via a Ni(I) oxidative addition to aryl iodides and, second, because the reported substrate scope includes reaction yields ranging from 14 to 85% that would potentially enable statistical modeling. Indeed, using MLR, we found that the yields of this reaction correlated with predicted oxidative addition rates (k_{pred}) and the buried volume of the aryl iodide substrate (% VBur_{2.0}) (Figure 7B). The fact that the k_{pred} correlates with reaction yield provides support for the proposed involvement of Ni(I) oxidative addition in the catalytic reaction. Moreover, the negative correlation of oxidative addition rates with the NMR yield indicates that the oxidative addition step in this reaction is not likely to be turnover-limiting. A decrease in yield for the aryl iodides with a faster oxidative addition rate could potentially be due to competitive side reactions such as homocoupling or protodehalogenation of aryl iodides. Furthermore, while the negative correlation with the buried volume term is more complicated to interpret, it supports that product formation depends on the

substrate's sterics, with more sterically demanding substrates leading to lower yields. Consequently, our analysis demonstrates the value of understanding kinetic trends for interpreting reactivity in catalysis, and we anticipate further use of this prediction platform in new catalyst optimization campaigns.

CONCLUSIONS

In this study, we have investigated the oxidative addition of aryl iodides by Ni(I) complexes supported by four catalytically important ligands. Through a combination of electroanalytical and statistical modeling techniques, kinetic profiling of various substrates and ligands was conducted, identifying the critical features of the oxidative addition process. These findings further enabled a mechanistic disparity of oxidative addition pathways for BPP-type ligands compared to other bi- and tridentate nitrogen-based ligands evaluated in the study. It also allowed extrapolation of oxidative addition rates, resulting in the creation of a heat map for the commercially available aryl iodides. Moreover, a case study of a Ni-catalyzed cross-coupling reaction demonstrated that the predicted oxidative addition rates can be utilized to interpret observed reactivities and rationalize the mechanism. We envision that the predictive models and mechanistic insight gained in this study will guide the design of new catalysts and catalytic reactions.

ASSOCIATED CONTENT

Supporting Information

The Supporting Information is available free of charge at <https://pubs.acs.org/doi/10.1021/jacs.3c01726>.

Heat map (ZIP)

Tabulated properties for heat map (XLSX)

Materials and methods; experimental cyclic voltammograms and kinetic data; parameters used in the modeling; experimental procedures; characterization data and spectra for the synthesis of ligands, substrates, and complexes; and coordinates of DFT-optimized structures (PDF)

AUTHOR INFORMATION

Corresponding Authors

Abigail G. Doyle – Department of Chemistry and Biochemistry, University of California, Los Angeles, California 90095, United States; orcid.org/0000-0002-6641-0833; Email: sigman@chem.utah.edu

Matthew S. Sigman – Department of Chemistry, University of Utah, Salt Lake City, Utah 84112, United States; orcid.org/0000-0002-5746-8830; Email: agdoyle@chem.ucla.edu

Authors

Tianhua Tang – Department of Chemistry, University of Utah, Salt Lake City, Utah 84112, United States

Avijit Hazra – Department of Chemistry, University of Utah, Salt Lake City, Utah 84112, United States; orcid.org/0000-0002-1102-8581

Daniel S. Min – Department of Chemistry and Biochemistry, University of California, Los Angeles, California 90095, United States

Wendy L. Williams – Department of Chemistry and Biochemistry, University of California, Los Angeles, California 90095, United States; Department of Chemistry, Princeton University, Princeton, New Jersey 08544, United States; orcid.org/0000-0003-2227-0856

Eli Jones – Department of Chemistry, University of Utah, Salt Lake City, Utah 84112, United States; orcid.org/0000-0003-4381-7427

Complete contact information is available at: <https://pubs.acs.org/10.1021/jacs.3c01726>

Author Contributions

[†]T.T. and A.H. contributed equally.

Notes

The authors declare no competing financial interest. The data that support the findings in this work are available within the paper and [Supporting Information](#).

ACKNOWLEDGMENTS

Research in the Sigman lab was supported by the National Science Foundation Center for Synthetic Organic Electrochemistry (CHE-2002158). NMR results included in this report were recorded at the David M. Grant NMR Center, a University of Utah Core Facility. Funds for the construction of the Center and the helium recovery system were obtained from the University of Utah and the National Institutes of Health awards 1C06RR017539-01A1 and 3R01GM063540-17W1, respectively. NMR instruments were purchased with the support of the University of Utah and the National Institutes of Health award 1S10OD25241-01. The Doyle group acknowledges financial support from NIGMS (R35 GM126986). The aryl iodide calculations used for the UMAP were performed using computational resources managed and supported by Princeton Research Computing.

REFERENCES

- (1) Goldfogel, M. J.; Huang, L.; Weix, D. J. Cross-electrophile Coupling: Principles and New Reactions. *Nickel Catalysis in Organic Synthesis*; Wiley January, 2020; Vol. 28, pp 183–222.
- (2) Tasker, S. Z.; Standley, E. A.; Jamison, T. F. Recent Advances in Homogeneous Nickel Catalysis. *Nature* **2014**, *509*, 299–309.

- (3) Twilton, J.; Le, C.; Zhang, P.; Shaw, M. H.; Evans, R. W.; MacMillan, D. W. C. The Merger of Transition Metal and Photocatalysis. *Nat. Rev. Chem* **2017**, *1*, 0052.

- (4) Richmond, E.; Moran, J. Recent Advances in Nickel Catalysis Enabled by Stoichiometric Metallic Reducing Agents. *Synthesis* **2018**, *50*, 499–513.

- (5) Milligan, J. A.; Phelan, J. P.; Badir, S. O.; Molander, G. A. Alkyl Carbon-Carbon Bond Formation by Nickel/Photoredox Cross-Coupling. *Angew. Chem., Int. Ed.* **2019**, *58*, 6152–6163.

- (6) Chan, A. Y.; Perry, I. B.; Bissonnette, N. B.; Buksh, B. F.; Edwards, G. A.; Frye, L. I.; Garry, O. L.; Lavagnino, M. N.; Li, B. X.; Liang, Y.; Mao, E.; Millet, A.; Oakley, J. V.; Reed, N. L.; Sakai, H. A.; Seath, C. P.; MacMillan, D. W. C. Metal-Photoredox: The Merger of Photoredox and Transition Metal Catalysis. *Chem. Rev.* **2022**, *122*, 1485–1542.

- (7) Malapit, C. A.; Prater, M. B.; Cabrera-Pardo, J. R.; Li, M.; Pham, T. D.; McFadden, T. P.; Blank, S.; Minter, S. D. Advances on the Merger of Electrochemistry and Transition Metal Catalysis for Organic Synthesis. *Chem. Rev.* **2022**, *122*, 3180–3218.

- (8) Kehoe, R.; Mahadevan, M.; Manzoora, A.; McMurray, G.; Wienefeld, P.; Baird, M. C.; Budzelaar, P. H. M. Reactions of the Ni(0) Compound Ni(PPh₃)₄ with Unactivated Alkyl Halides: Oxidative Addition Reactions Involving Radical Processes and Nickel(I) Intermediates. *Organometallics* **2018**, *37*, 2450–2467.

- (9) Bajo, S.; Laidlaw, G.; Kennedy, A. R.; Sproules, S.; Nelson, D. J. Oxidative Addition of Aryl Electrophiles to a Prototypical Nickel(0) Complex: Mechanism and Structure/Reactivity Relationships. *Organometallics* **2017**, *36*, 1662–1672.

- (10) Greaves, M. E.; Johnson Humphrey, E. L. B.; Nelson, D. J. Reactions of Nickel(0) with Organochlorides, Organobromides, and Organoiodides: Mechanisms and Structure/Reactivity Relationships. *Catal. Sci. Technol.* **2021**, *11*, 2980–2996.

- (11) For select reviews, see (a) Lin, C.-Y.; Power, P. P. Complexes of Ni(I): A “Rare” Oxidation State of Growing Importance. *Chem. Soc. Rev.* **2017**, *46*, 5347–5399. (b) Bismuto, A.; Finkelstein, P.; Müller, P.; Morandi, B. The Journey of Ni(I) Chemistry. *Helv. Chim. Acta* **2021**, *104*, No. e2100177.

- (12) Colon, I.; Kelsey, D. R. Coupling of Aryl Chlorides by Nickel and Reducing Metals. *J. Org. Chem.* **1986**, *51*, 2627–2637.

- (13) Oderinde, M. S.; Frenette, M.; Robbins, D. W.; Aquila, B.; Johannes, J. W. Photoredox Mediated Nickel Catalyzed Cross-Coupling of Thiols with Aryl and Heteroaryl Iodides via Thiyl Radicals. *J. Am. Chem. Soc.* **2016**, *138*, 1760–1763.

- (14) Shevick, S. L.; Obradors, C.; Shenvi, R. A. Mechanistic Interrogation of Co/Ni-Dual Catalyzed Hydroarylation. *J. Am. Chem. Soc.* **2018**, *140*, 12056–12068.

- (15) Kawamata, Y.; Vantourout, J. C.; Hickey, D. P.; Bai, P.; Chen, L.; Hou, Q.; Qiao, W.; Barman, K.; Edwards, M. A.; Garrido-Castro, A. F.; deGruyter, J. N.; Nakamura, H.; Knouse, K.; Qin, C.; Clay, K. J.; Bao, D.; Li, C.; Starr, J. T.; Garcia-Irizarry, C.; Sach, N.; White, H. S.; Neurock, M.; Minter, S. D.; Baran, P. S. Electrochemically Driven, Ni-Catalyzed Aryl Amination: Scope, Mechanism, and Applications. *J. Am. Chem. Soc.* **2019**, *141*, 6392–6402.

- (16) Lou, T. S.-B.; Kawamata, Y.; Ewing, T.; Correa-Otero, G. A.; Collins, M. R.; Baran, P. S. Scalable, Chemoselective Nickel Electrocatalytic Sulfonylation of Aryl Halides with SO₂. *Angew. Chem., Int. Ed.* **2022**, *61*, No. e202208080.

- (17) Wang, Y.; Zhang, X.; Liu, H.; Chen, H.; Huang, D. Nickel-Catalyzed Direct Formation of the C–S Bonds of Aryl Sulfides from Arylsulfonyl Chlorides and Aryl Iodides Using Mn as a Reducing Agent. *Org. Chem. Front.* **2017**, *4*, 31–36.

- (18) Matsubara, K.; Yamamoto, H.; Miyazaki, S.; Inatomi, T.; Nonaka, K.; Koga, Y.; Yamada, Y.; Veiros, L. F.; Kirchner, K. Dinuclear Systems in the Efficient Nickel-Catalyzed Kumada–Tamao–Corriu Cross-Coupling of Aryl Halides. *Organometallics* **2017**, *36*, 255–265.

- (19) Inatomi, T.; Fukahori, Y.; Yamada, Y.; Ishikawa, R.; Kanegawa, S.; Koga, Y.; Matsubara, K. Ni(I)–Ni(III) Cycle in Buchwald–

Hartwig Amination of Aryl Bromide Mediated by NHC-Ligated Ni(I) Complexes. *Catal. Sci. Technol.* **2019**, *9*, 1784–1793.

(20) Ting, S. I.; Williams, W. L.; Doyle, A. G. Oxidative Addition of Aryl Halides to a Ni(I)-Bipyridine Complex. *J. Am. Chem. Soc.* **2022**, *144*, 5575–5582.

(21) Qin, Y.; Sun, R.; Gianoulis, N. P.; Nocera, D. G. Photoredox Nickel-Catalyzed C-S Cross-Coupling: Mechanism, Kinetics, and Generalization. *J. Am. Chem. Soc.* **2021**, *143*, 2005–2015.

(22) Till, N. A.; Oh, S.; MacMillan, D. W. C.; Bird, M. J. The Application of Pulse Radiolysis to the Study of Ni(I) Intermediates in Ni-Catalyzed Cross-Coupling Reactions. *J. Am. Chem. Soc.* **2021**, *143*, 9332–9337.

(23) Sun, R.; Qin, Y.; Rucolo, S.; Schnedermann, C.; Costentin, C.; Nocera, D. G. Elucidation of a Redox-Mediated Reaction Cycle for Nickel-Catalyzed Cross Coupling. *J. Am. Chem. Soc.* **2019**, *141*, 89–93.

(24) Lin, Q.; Diao, T. Mechanism of Ni-Catalyzed Reductive 1,2-Dicarbonylfunctionalization of Alkenes. *J. Am. Chem. Soc.* **2019**, *141*, 17937–17948.

(25) Wagner, C. L.; Herrera, G.; Lin, Q.; Hu, C. T.; Diao, T. Redox Activity of Pyridine-Oxazoline Ligands in the Stabilization of Low-Valent Organonickel Radical Complexes. *J. Am. Chem. Soc.* **2021**, *143*, 5295–5300.

(26) Ju, L.; Lin, Q.; LiBretto, N. J.; Wagner, C. L.; Hu, C. T.; Miller, J. T.; Diao, T. Reactivity of (Bi-Oxazoline)Organonickel Complexes and Revision of a Catalytic Mechanism. *J. Am. Chem. Soc.* **2021**, *143*, 14458–14463.

(27) Till, N. A.; Tian, L.; Dong, Z.; Scholes, G. D.; MacMillan, D. W. C. Mechanistic Analysis of Metallaphotoredox C-N Coupling: Photocatalysis Initiates and Perpetuates Ni(I)/Ni(III) Coupling Activity. *J. Am. Chem. Soc.* **2020**, *142*, 15830–15841.

(28) Na, H.; Mirica, L. M. Deciphering the Mechanism of the Ni-Photocatalyzed C–O Cross-Coupling Reaction Using a Tridentate Pyridinophane Ligand. *Nat. Commun.* **2022**, *13*, 1313.

(29) Barrios-Landeros, F.; Carrow, B. P.; Hartwig, J. F. Effect of Ligand Steric Properties and Halide Identity on the Mechanism for Oxidative Addition of Haloarenes to Trialkylphosphine Pd(0) Complexes. *J. Am. Chem. Soc.* **2009**, *131*, 8141–8154.

(30) Newman-Stonebraker, S. H.; Smith, S. R.; Borowski, J. E.; Peters, E.; Gensch, T.; Johnson, H. C.; Sigman, M. S.; Doyle, A. G. Univariate Classification of Phosphine Ligation State and Reactivity in Cross-Coupling Catalysis. *Science* **2021**, *374*, 301–308.

(31) Zhang, B.; Gao, Y.; Hioki, Y.; Oderinde, M. S.; Qiao, J. X.; Rodriguez, K. X.; Zhang, H.-J.; Kawamata, Y.; Baran, P. S. Ni-Electrocatalytic Csp³-Csp³ Doubly Decarboxylative Coupling. *Nature* **2022**, *606*, 313–318.

(32) Lin, Q.; Fu, Y.; Liu, P.; Diao, T. Monovalent Nickel-Mediated Radical Formation: A Concerted Halogen-Atom Dissociation Pathway Determined by Electroanalytical Studies. *J. Am. Chem. Soc.* **2021**, *143*, 14196–14206.

(33) Hickey, D. P.; Sandford, C.; Rhodes, Z.; Gensch, T.; Fries, L. R.; Sigman, M. S.; Minter, S. D. Investigating the Role of Ligand Electronics on Stabilizing Electrocatalytically Relevant Low-Valent Co(I) Intermediates. *J. Am. Chem. Soc.* **2019**, *141*, 1382–1392.

(34) Sandford, C.; Fries, L. R.; Ball, T. E.; Minter, S. D.; Sigman, M. S. Mechanistic Studies into the Oxidative Addition of Co(I) Complexes: Combining Electroanalytical Techniques with Parameterization. *J. Am. Chem. Soc.* **2019**, *141*, 18877–18889.

(35) Tang, T.; Sandford, C.; Minter, S. D.; Sigman, M. S. Analyzing mechanisms in Co(I) redox catalysis using a pattern recognition platform. *Chem. Sci.* **2021**, *12*, 4771–4778.

(36) Tang, T.; Friede, N. C.; Minter, S. D.; Sigman, M. S. Comparing Halogen Atom Abstraction Kinetics for Mn(I), Fe(I), Co(I), and Ni(I) Complexes by Combining Electroanalytical and Statistical Modeling. *Eur. J. Org. Chem.* **2022**, *2022*, No. e202200064.

(37) Sandford, C.; Edwards, M. A.; Klunder, K. J.; Hickey, D. P.; Li, M.; Barman, K.; Sigman, M. S.; White, H. S.; Minter, S. D. A synthetic chemist's guide to electroanalytical tools for studying reaction mechanisms. *Chem. Sci.* **2019**, *10*, 6404–6422.

(38) Tang, T.; Jones, E.; Wild, T.; Hazra, A.; Minter, S. D.; Sigman, M. S. Investigating Oxidative Addition Mechanisms of Allylic Electrophiles with Low-Valent Ni/Co Catalysts Using Electroanalytical and Data Science Techniques. *J. Am. Chem. Soc.* **2022**, *144*, 20056–20066.

(39) Ligands with a chiral oxazoline backbone, such as bis-oxazoline (BOX or BiOX) and pyridine-oxazoline (Pyrox) ligands, were also reported to activate aryl iodides in catalysis. The studies of these ligands' performance in oxidative addition are underway. For studies with BOX, BiOX, or Pyrox ligands, see (a) Jin, Y.; Fan, P.; Wang, C. Nickel-Catalyzed Reductive Asymmetric Aryl-Acylation and Aryl-Carbonylation of Unactivated Alkenes. *CCS Chem.* **2022**, *4*, 1510–1518. (b) Poremba, K. E.; Dibrell, S. E.; Reisman, S. E. Nickel-Catalyzed Enantioselective Reductive Cross-Coupling Reactions. *ACS Catal.* **2020**, *10*, 8237–8246.

(40) Sun, G.-Q.; Zhang, W.; Liao, L.-L.; Li, L.; Nie, Z.-H.; Wu, J.-G.; Zhang, Z.; Yu, D.-G. Nickel-Catalyzed Electrochemical Carboxylation of Unactivated Aryl and Alkyl Halides with CO₂. *Nat. Commun.* **2021**, *12*, 7086.

(41) Wu, F.; Wang, W.; Yao, K. Nickel-Catalyzed Reductive Cross-Coupling of Benzylic Sulfonium Salts with Aryl Iodides. *Synlett* **2022**, *33*, 361–366.

(42) Everson, D. A.; Shrestha, R.; Weix, D. J. Nickel-Catalyzed Reductive Cross-Coupling of Aryl Halides with Alkyl Halides. *J. Am. Chem. Soc.* **2010**, *132*, 920–921.

(43) Biswas, S.; Weix, D. J. Mechanism and Selectivity in Nickel-Catalyzed Cross-Electrophile Coupling of Aryl Halides with Alkyl Halides. *J. Am. Chem. Soc.* **2013**, *135*, 16192–16197.

(44) Pan, Y.; Gong, Y.; Song, Y.; Tong, W.; Gong, H. Deoxygenative Cross-Electrophile Coupling of Benzyl Chloroformates with Aryl Iodides. *Org. Biomol. Chem.* **2019**, *17*, 4230–4233.

(45) Shrestha, R.; Dorn, S. C. M.; Weix, D. J. Nickel-Catalyzed Reductive Conjugate Addition to Enones via Allylnickel Intermediates. *J. Am. Chem. Soc.* **2013**, *135*, 751–762.

(46) Chen, H.; Yue, H.; Zhu, C.; Rueping, M. Reactivity in Nickel-Catalyzed Multi-Component Sequential Reductive Cross-Coupling Reactions. *Angew. Chem., Int. Ed.* **2022**, *61*, No. e202204144.

(47) Zou, Z.; Li, H.; Huang, M.; Zhang, W.; Zhi, S.; Wang, Y.; Pan, Y. Electrochemical-Promoted Nickel-Catalyzed Oxidative Fluoroalkylation of Aryl Iodides. *Org. Lett.* **2021**, *23*, 8252–8256.

(48) Joshi-Pangu, A.; Ganesh, M.; Biscoe, M. R. Nickel-Catalyzed Negishi Cross-Coupling Reactions of Secondary Alkylzinc Halides and Aryl Iodides. *Org. Lett.* **2011**, *13*, 1218–1221.

(49) Ni, S.; Zhang, W.; Mei, H.; Han, J.; Pan, Y. Ni-Catalyzed Reductive Cross-Coupling of Amides with Aryl Iodide Electrophiles via C-N Bond Activation. *Org. Lett.* **2017**, *19*, 2536–2539.

(50) Le Vaillant, F.; Mateos Calbet, A.; González-Pelayo, S.; Reijerse, E. J.; Ni, S.; Busch, J.; Cornella, J. Catalytic Synthesis of Phenols with Nitrous Oxide. *Nature* **2022**, *604*, 677–683.

(51) Arendt, K. M.; Doyle, A. G. Dialkyl Ether Formation by Nickel-Catalyzed Cross-Coupling of Acetals and Aryl Iodides. *Angew. Chem., Int. Ed.* **2015**, *54*, 9876–9880.

(52) Nallagonda, R.; Musaev, D. G.; Karimov, R. R. Light-Promoted Dearomative Cross-Coupling of Heteroarene Salts and Aryl Iodides via Nickel Catalysis. *ACS Catal.* **2022**, *12*, 1818–1829.

(53) Jiao, K.-J.; Ma, C.; Liu, D.; Qiu, H.; Cheng, B.; Mei, T.-S. Nickel-Catalyzed Electrochemical Reductive Relay Cross-Coupling of Alkyl Halides with Alkyl Carboxylic Acids. *Org. Chem. Front.* **2021**, *8*, 6603–6608.

(54) Kumar, G. S.; Peshkov, A.; Brzozowska, A.; Nikolaienko, P.; Zhu, C.; Rueping, M. Nickel-catalyzed Chain-walking Cross-electrophile Coupling of Alkyl and Aryl Halides and Olefin Hydroarylation Enabled by Electrochemical Reduction. *Angew. Chem., Int. Ed.* **2020**, *59*, 6513–6519.

(55) Jiao, K.-J.; Liu, D.; Ma, H.-X.; Qiu, H.; Fang, P.; Mei, T.-S. Nickel-catalyzed Electrochemical Reductive Relay Cross-coupling of Alkyl Halides to Aryl Halides. *Angew. Chem., Int. Ed.* **2020**, *59*, 6520–6524.

(56) Diccianni, J.; Lin, Q.; Diao, T. Mechanisms of Nickel-Catalyzed Coupling Reactions and Applications in Alkene Functionalization. *Acc. Chem. Res.* **2020**, *53*, 906–919.

(57) Hansch, C.; Leo, A.; Taft, R. W. A survey of Hammett substituent constants and resonance and field parameters. *Chem. Rev.* **1991**, *91*, 165–195.

(58) Portnoy, M.; Milstein, D. Mechanism of Aryl Chloride Oxidative Addition to Chelated Palladium(0) Complexes. *Organometallics* **1993**, *12*, 1665–1673.

(59) Tsou, T. T.; Kochi, J. K. Mechanism of Oxidative Addition. Reaction of Nickel(0) Complexes with Aromatic Halides. *J. Am. Chem. Soc.* **1979**, *101*, 6319–6332.

(60) Amatore, C.; Pfluger, F. Mechanism of Oxidative Addition of Palladium(0) with Aromatic Iodides in Toluene, Monitored at Ultramicroelectrodes. *Organometallics* **1990**, *9*, 2276–2282.

(61) Biscoe, M. R.; Fors, B. P.; Buchwald, S. L. A New Class of Easily Activated Palladium Precatalysts for Facile C–N Cross-Coupling Reactions and the Low Temperature Oxidative Addition of Aryl Chlorides. *J. Am. Chem. Soc.* **2008**, *130*, 6686–6687.

(62) Wong, C. L.; Kochi, J. K. Electron Transfer with Organometals. Steric Effects as Probes for Outer-Sphere and Inner-Sphere Oxidations of Homoleptic Alkylmetals with Iron(III) and Iridate(IV) Complexes. *J. Am. Chem. Soc.* **1979**, *101*, 5593–5603.

(63) Harper, K. C.; Sigman, M. S. Using Physical Organic Parameters To Correlate Asymmetric Catalyst Performance. *J. Org. Chem.* **2013**, *78*, 2813–2818.

(64) Sigman, M. S.; Harper, K. C.; Bess, E. N.; Milo, A. The Development of Multidimensional Analysis Tools for Asymmetric Catalysis and Beyond. *Acc. Chem. Res.* **2016**, *49*, 1292–1301.

(65) (a) McInnes, L.; Healy, J.; Melville, J. UMAP: Uniform Manifold Approximation and Projection for Dimension Reduction. 2018-02-09, arXiv:1802.03426. <https://arxiv.org/abs/1802.03426> (accessed 2021-05-15) (b) McInnes, L.; Healy, J.; Saul, N.; Großberger, L. UMAP: Uniform Manifold Approximation and Projection. *J. Open Source Softw.* **2018**, *3*, 861.

(66) percent buried volume" (%Vbur) is defined as the percent of the total volume of a defined sphere occupied by the molecule. It was calculated with a radius specified in the manuscript using the DBSTEP script from: Luchini, G.; Paton, R. S. *DBSTEP: DFT Based Steric Parameters*, 2021.10.5281/zenodo.4702097.

(67) Kariofillis, S. K.; Jiang, S.; Żurański, A. M.; Gandhi, S. S.; Martinez Alvarado, J. I.; Doyle, A. G. Using Data Science to Guide Aryl Bromide Substrate Scope Analysis in a Ni/Photoredox-Catalyzed Cross-Coupling with Acetals as Alcohol-Derived Radical Sources. *J. Am. Chem. Soc.* **2022**, *144*, 1045–1055.

(68) Lu, J.; Donnecke, S.; Paci, I.; Leitch, D. C. A Reactivity Model for Oxidative Addition to Palladium Enables Quantitative Predictions for Catalytic Cross-Coupling Reactions. *Chem. Sci.* **2022**, *13*, 3477–3488.